LIMIT CYCLES OF A FLEXIBLE SHAFT

WITH HYDRODYNAMIC JOURNAL BEARINGS IN UNSTABLE REGIMES

R. David Brown and Henry F. Black (deceased)
Mechanical Engineering Department,
Heriot-Watt University, Edinburgh, Scotland, U.K.

SUMMARY

A simple linear stability criterion demonstrates that an increase in shaft flexibility results in reduced stability. An examination of the corresponding complex eigenvalues confirms the stability reduction but also shows that the maximum negative damping in flexible shafts/bearing systems is very small. Thus the energy transferred to the shaft whirl through the lubricant film is also very small.

A non-linear behaviour in these cases can be investigated if appropriate solutions of Reynolds equation are available. An approximate but realistic method has been incorporated into a dynamic simulation. It is demonstrated that in unstable regimes, flexible shafts have small limit cycle motions.

INTRODUCTION

In the last decade several papers have been published dealing with the transient response of rotor bearing systems, e.g. Kirk (ref. 1) and Childs (ref. 2).

McCallion (ref. 3), Myrick and Rylander (ref. 8), used a finite difference approach to obtain instantaneous bearing forces. Because of the complexity of the oil film simulation both papers used a 3 mass symmetrical model and were mainly concerned with establishing the validity of the method rather than using it in a systematic way.

The influence of shaft flexibility on instability onset speed has been examined by Dostal et al. (ref. 5) and Ruhl (ref. 4). In both these papers a multi-degree of freedom representation of the shaft was coupled with a short bearing representation of the oil forces. However it was clearly demonstrated that for a flexible shaft there was a drastic reduction in the stability boundary.

An almost universal solution to unstable circular bearings is to replace them with 4 fixed lobe or tilting pad bearings. While tilting pad bearings are superior from a linear stability viewpoint Greathead (ref. 6) has pointed out an increase in resonant response due to reduced damping. It was also demonstrated that a subsynchronous vibration due to steam gland forces

increased in severity. Now practical experience with tilting
pad bearings has raised some doubts over mechanical reliability
of the pad pivots. Thus the advantages of tilting pad bearings
may be less than generally assumed.

The work described below deals with a symmetric 3 mass rotor
supported on hydrodynamic bearings. An approximate method of
representing finite bearings is used to calculate bearing forces.
As the method sums forces from a number of independent circular
lobes lemon 3 and 4 lobe bearings can be taken into account.
The calculations in this paper are based on an axial groove
bearing as this is likely to have less stability. Linear
analysis precedes non-linear simulation of some unstable
conditions. The demonstration of small limit cycles suggests
that necessarily flexible rotors e.g. helicopter tail rotors may
be practical without either tilt pad bearings or external
dampers.

<div align="center">SYMBOLS</div>

C	radial clearance
e	journal eccentricity ratio
F	bearing force
H	non-dimensional film gap $(1 + e \cos \theta)$
K	half shaft stiffness; bearing stiffness
L	bearing length
M	half central mass
m	bearing mass
P	dimensionless pressure, $\dfrac{P}{\mu\omega} (C/R)^2$
R	bearing radius
X,x	mid-span and bearing horizontal motion
Y,y	midspan and bearing vertical motion
Δ	geometrical eccentricity of masses
ξ	non-dimensionalised bearing axial distance
θ	film co-ordinate
$\dot{\phi}$	angular velocity of journal/bearing line of centres

μ viscosity

ω angular velocity of journal

HYDRODYNAMIC BEARING FORCES

Reynolds lubrication equation for constant viscosity conditions can be written as

$$\frac{\partial}{\partial\theta}(H^3 \frac{\partial P}{\partial\theta}) + \frac{R^2}{L^2} \frac{\partial}{\partial\xi}(H^3 \frac{\partial P}{\partial\xi}) = 6e \sin\theta (1-2\dot\phi/\omega) + 12\dot e/_\omega \cos\theta \qquad (1)$$

If the axial pressure distribution in an aligned bearing is assumed to be parabolic and symmetric about the mid plane

$$P = 4 P_{max} \xi (1-\xi)$$

Reynolds equation can then be written in terms of the mean axial pressure $\bar P$

$$\frac{d}{d\theta}(H^3 \frac{d\bar P}{d\theta}) - 12 \frac{R^2}{L^2} H^3 \bar P = 6e \sin\theta (1-2\dot\phi/\omega) + 12 e/_\omega \cos\theta \qquad (2)$$

An approximate solution can be obtained using the Galerkin technique to minimise the mean square error. In this case only a single approximating function was used, the long bearing solution to equation (1). The approximation is substituted into equation (2) and integrated after multiplication by the long bearing solution. The resulting scaling factor is less than one and can be considered as a leakage correction factor.

The pressure distribution obtained needs to be integrated to obtain the required force components. Traditionally Simpson's rule is used for numerical integration of bearing pressures but a Gaussian method is more efficient.

As the method is recognised to be approximate likely errors in the vector forces need to be assessed. A detailed comparison for static loads and dynamic coefficients for a lemon bore bearing was presented by Black and Brown (ref. 7). Some results for an axial groove bearing are given here (figs. 2,4,5). These comparisons are based on either static conditions or vanishingly small velocity perturbations for the damping coefficients.

Squeeze film effects were calculated and compared for an 180° arc bearing. The comparison between the approximate method and a finite difference method (fig. 3) demonstrates that sufficient accuracy is achieved for dynamic simulation.

The simplest model of a realistic shaft (fig. 1) consists of a 3 mass rotor supported in hydrodynamic bearings. By taking advantage of an assumed symmetry, McCallion (ref. 3), the equations of motion can be written in spaced fixed coordinates (fig. 1):

$$[M]\{\ddot{x}\} + [C]\{\dot{x}\} + [K]\{x\} = 0 \text{ for free motion} \tag{3}$$

where

$$M = \begin{bmatrix} M & O & O & O \\ O & M & O & O \\ O & O & m & O \\ O & O & O & m \end{bmatrix} \qquad K = \begin{bmatrix} K & O & -K & O \\ O & K & O & -K \\ -K & O & K+K_{xx} & K_{xy} \\ -O & -K & K_{xy} & K+K_{yy} \end{bmatrix}$$

$$C = \begin{bmatrix} B & O & O & O \\ O & B & O & O \\ O & O & B_{xx} & B_{xy} \\ O & O & B_{yx} & B_{yy} \end{bmatrix} \text{ and } x = \begin{Bmatrix} X \\ Y \\ x \\ y \end{Bmatrix}$$

Following Ruhl (ref. 4) equations (1) can be expanded into 8, 1st order equations.

Thus

$$\begin{bmatrix} M & O \\ O & I \end{bmatrix} \begin{Bmatrix} \ddot{x} \\ \dot{x} \end{Bmatrix} + \begin{bmatrix} C & K \\ -I & O \end{bmatrix} \begin{Bmatrix} \dot{x} \\ x \end{Bmatrix} = 0$$

and assuming $x = q\,e^{st}$

$$\lambda \begin{Bmatrix} \dot{x} \\ x \end{Bmatrix} = \begin{bmatrix} -M^{-1}C & -M^{-1}K \\ I & O \end{bmatrix} \begin{Bmatrix} \dot{x} \\ x \end{Bmatrix} \tag{4}$$

where

$$M^{-1}C = \begin{bmatrix} B/M & O & O & O \\ O & B/M & O & O \\ O & O & B_{xx} & B_{xy}/m \\ O & O & B_{yx}/m & B_{yy}/m \end{bmatrix}$$

$$M^{-1}K = \begin{bmatrix} K/M & 0 & -K/M & 0 \\ 0 & K/M & 0 & -K/M \\ -K/M & 0 & \dfrac{K+K_{xx}}{m} & K_{xy}/m \\ 0 & -K/m & K_{xy}/m & \dfrac{K+K_{yy}}{m} \end{bmatrix}$$

Equation (4) is a standard eigenvalue problem where roots can be obtained using a library sub-routine. The roots will occur in complex conjugate pairs $s_i = \lambda_i \pm j\Omega_i$ or as real roots.

The stability boundary can be established by examining the variation in the real part λ_i of each root as a function of an operating parameter. For stable operation all λ_i must be negative and when any λ_i becomes positive the model becomes unstable.

However the sensitivity of the growth (or decay) factor to operating variables near the stability boundary has not often been investigated in a systematic way. A conventional presentation of the stability for a flexible shaft, Dostal et al. (ref. 5) and Ruhl (ref. 4), has stability parameter plotted against bearing eccentricity for a range of shaft flexibilities. An example of such a stability plot is shown (fig. 6) for the lumped mass model (fig. 1) of Table 1.

Operating lines of constant viscosity are superimposed on the stability plot. These are obtained by noting that eccentricity is a function of Sommerfeld Number, which depends on the product of speed and viscosity for a fixed load and geometry. However, speed is already incorporated into the stability parameter and so operating lines can be presented as lines of constant viscosity.

The variation in the dominant eigenvalue near the stability boundary for a single viscosity (fig. 7) clearly shows the significant effect of shaft flexibility. With shaft flexibility low a small change in bearing eccentricity has a dramatic effect on the rate of decay. However, as the shaft flexibility increases there is a marked convergence of the lines of constant eccentricity. More significantly the region of coalescence moves closer to the stability boundary as flexibility increases.

Replacing the axial groove bearings of the model with lemon bore bearings (ref. 7) produces another stability plot (fig. 8). The stability is clearly much improved compared with axial groove bearings. Indeed for moderate to high flexibility ($C/_{\partial} < 1$) the shaft is completely stable.

These linear calculations demonstrate that in certain circumstances, unstable flexible shafts have very low negative damping. No external damping was included in these linear calculations so the results are pessimistic if no other destabilizing forces are present.

NON-LINEAR SIMULATION

The equations for free motion (equ. (3)) can be modified for forced vibration

Thus $[M] \{\ddot{x}\} + [C] \{\dot{x}\} + [K] \{x\} = e^{-i\omega t} \{M\Delta\} + \{F\}$

where $\{M\Delta\}$ is the mass eccentricity vector

and $\{F\}$ is bearing force vector

For numerical integration acceleration needs to be implicity defined.

Thus

$$\{\ddot{x}\} = [-M]^{-1} [C] \dot{x} - [M]^{-1} [K] x + \omega^2 \{\Delta\} + [M^{-1}]\{F\}$$

These 4 equations are reformed into a set of 8 first order equations and integrated using a 4th order Runge-Kutta method.

NUMERICAL RESULTS

The 3 mass shaft model (fig. 1) with axial groove bearings was used for non-linear simulation of some unstable cases. Initial vertical deflection of the central mass was set at its static value, all other deflections and velocities zero. For a flexible shaft $(C/_{\partial} = 0.1)$ with no external damping response, calculations for 12 shaft revolutions shown in figures 9 and 10 for a bearing position indicate limit cycles for zero unbalance and a large central unbalance respectively. However reflection on published work particularly that of Holmes (9) led to closer examination of the calculated results. At the end of the integration the growth rate (log dec) was around 0.0025, graphically insignificant. The calculations were extended with external damping added to the central mass. After some 60 shaft revolutions the undamped model response was increasing while with $\xi = 0.01$ damping maximum excursion at both shaft centre and bearing were reached after 30 revolutions.

Additional calculations were carried out for a stiffer shaft $(C/_{\partial} = 0.3)$ at a more unstable condition. The results for zero unbalance are summarised in fig. 11. An external damping ratio of 3% is needed before extreme excursion values of mid-span deflection are established after 15 shaft revolutions.

336

DISCUSSION AND CONCLUSIONS

It has been demonstrated that for an unstable flexible shaft the limit cycle motion can be small. These calculations were carried out for axial groove bearings with the addition of a small amount of external damping. The assumed additional damping was less than that used by McCallion (ref. 3). Further work using non-circular bearings for unstable conditions (e.g., fig. 8) is expected to demonstrate that unstable flexible shafts do not develop unacceptable levels of vibration.

TABLE 1.
3 MASS SHAFT WITH AXIAL GROOVE BEARINGS

HALF CENTRAL MASS	7.237 Kg
JOURNAL MASS	4.382 Kg
BEARING LENGTH	25.4 mm
BEARING DIAMETER	50.8 mm
BEARING DIAMETRAL CLEARANCE	50.8 μm

SHAFT FLEXIBILITY $C/_{\partial}$	0.1	0.3
SHAFT STIFFNESS K MN$/_m$	.279	.837
SPEED R.P.M.	7120	12,470
JOURNAL ECCENTRICITY	.41	0.29
CRITICAL MASS $_{\omega} \dfrac{C}{g}$	1.2	2.1

REFERENCES

1. Kirk, R.G.; Gunter, E.J.; Transient Response of Rotor-Bearing Systems. ASME Transactions. Journal of Engineering for Industry. May 1974 pp. 682-693.

2. Childs, D.W.; A Modal Transient Simulation Model for Flexible Asymmetric Rotors. ASME Transactions. Journal of Engineering for Industry 1976.

3. McCallion, H.; Wales, D.R.; The Influence of Oil Lubricated Bearings on the Dynamics of Rotating Systems. I.Mech.E. Proceedings Vol. 190 54/76.

4. Ruhl, R.L.; Booker, J.F.; A Finite Element Model for Distributed Parameter Turborotor Systems. ASME Transactions. Journal of Engineering for Industry. February 1972 pp. 126-132.

5. Dostal, M.; Roberts, J.B.; Holmes, R.; Stability Control of Flexible Shafts Supported on Oil-Film Bearings. Journal of Sound and Vibration 1974. Vol. 35 Pt. 3 pp. 361-377.

6. Greathead, S.H.; Bastow, P.; Investigations into Load Dependant Vibrations on the High Pressure Rotor on Large Turbo-Generators. Vibrations in Rotating Machinery. I.Mech.E. Conference, Cambridge 1976.

7. Black, H.F.; Brown, R.D.; Fast Dynamic Calculations for Non-Circular Bearings. I.Mech.E. Tribology Convention, Durham April 1976.

8. Myrick, S.T.; Rylander, H.G.; Analysis of Flexible Rotor Whirl Using A Realistic Hydrodynamic Journal Bearing. ASME Transactions. Journal of Engineering for Industry. November 1976 pp. 1135-44.

9. Holmes, R.; The Non-Linear Performance Of Turbine Bearings Journal of Mechanical Eng. Sc. Vol. 12 No.6 December 1970.
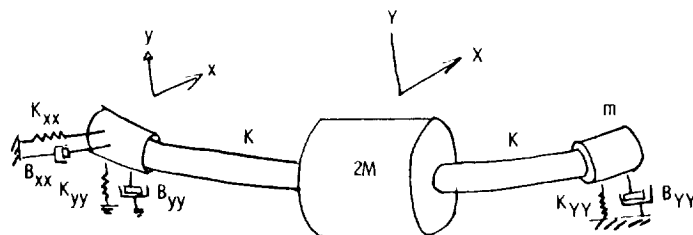
Figure 1. - Three-mass model.
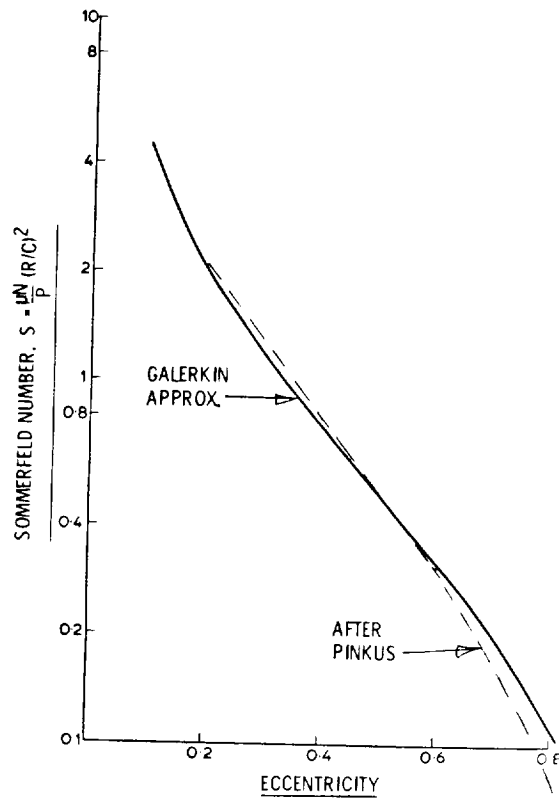
Figure 2. - Two-axial-groove bearing. L/D = 0.5.
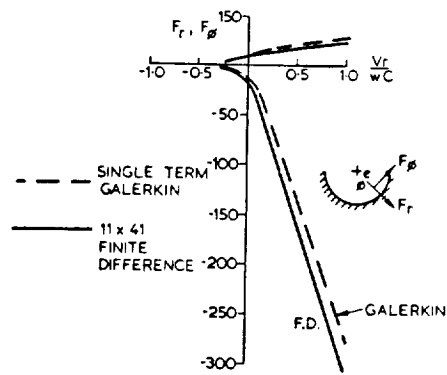
Figure 3. - Comparison of finite difference with an approximate method. Squeeze forces; L/D = 1; 180° arc; $\phi = 45^\circ$; $\varepsilon = 0.9$.

339
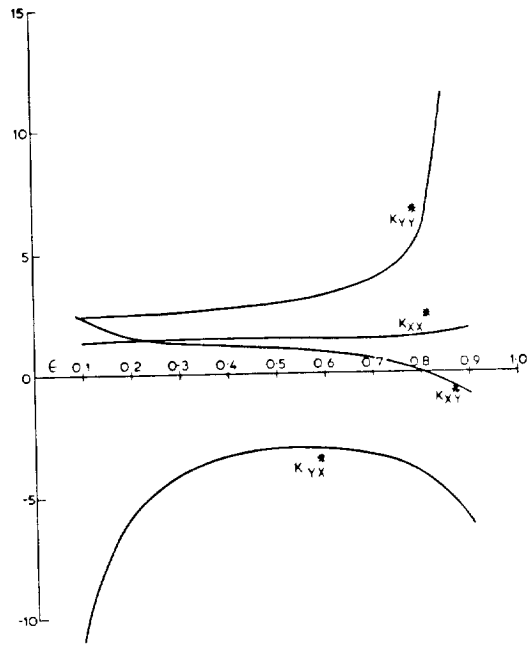
Figure 4. - Axial-groove bearing. L/D = 0.5; nondimen-
sionalized stiffness.
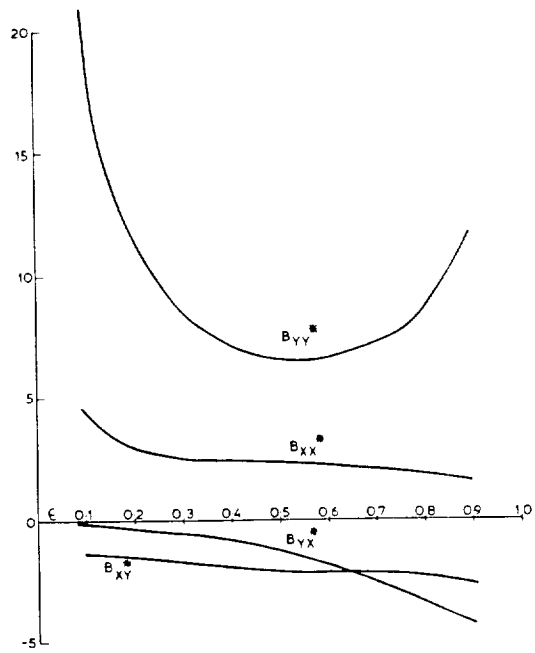
Figure 5. - Axial-groove bearing. L/D = 0.5; nondimen-
sionalized damping.

340
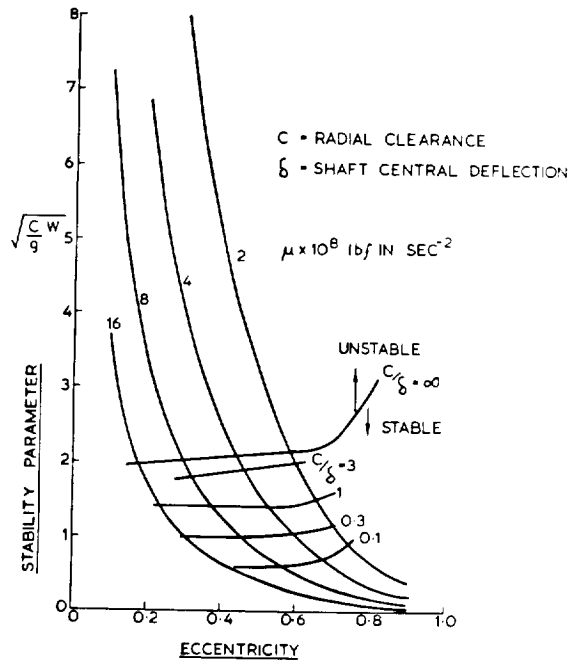
Figure 6. - Effect of stiffness on stability.
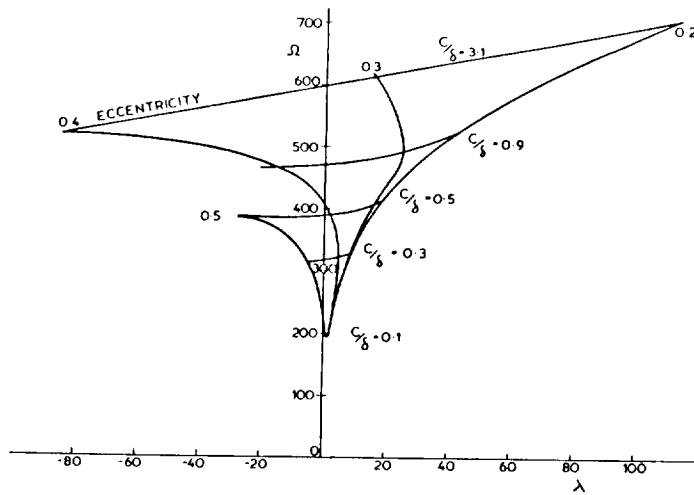
Figure 7. - Complex-plane dominant eigenvalue. Three-mass shift; $\mu = 8 \times 10^{-8}$ lbf in sec^{-2}; $x = Xe^{\lambda + i\Omega}$.
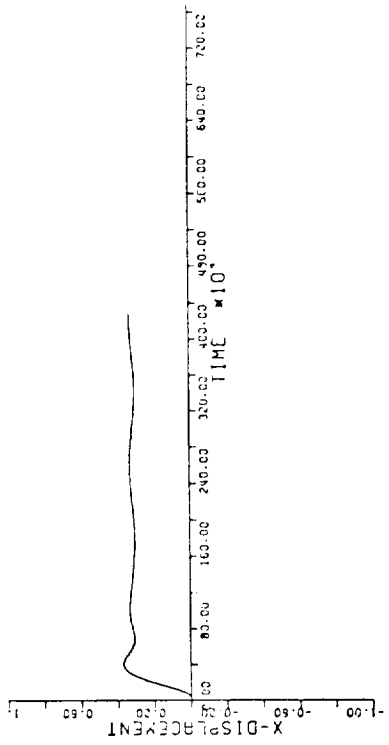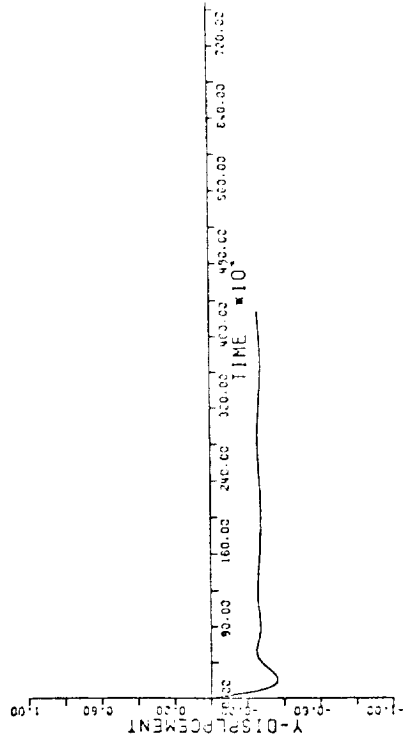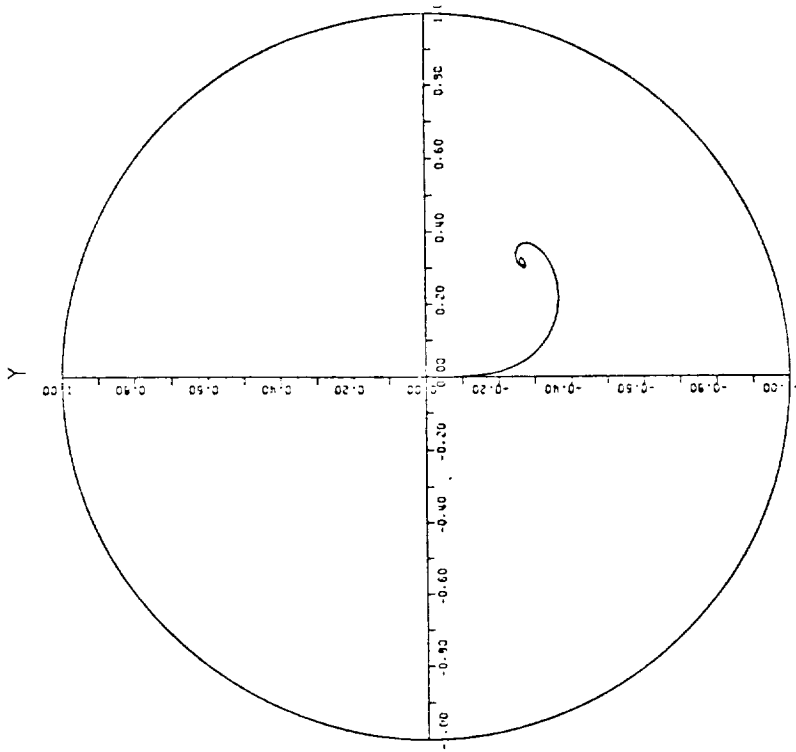
Figure 8. - Example of a flexible shaft.

342
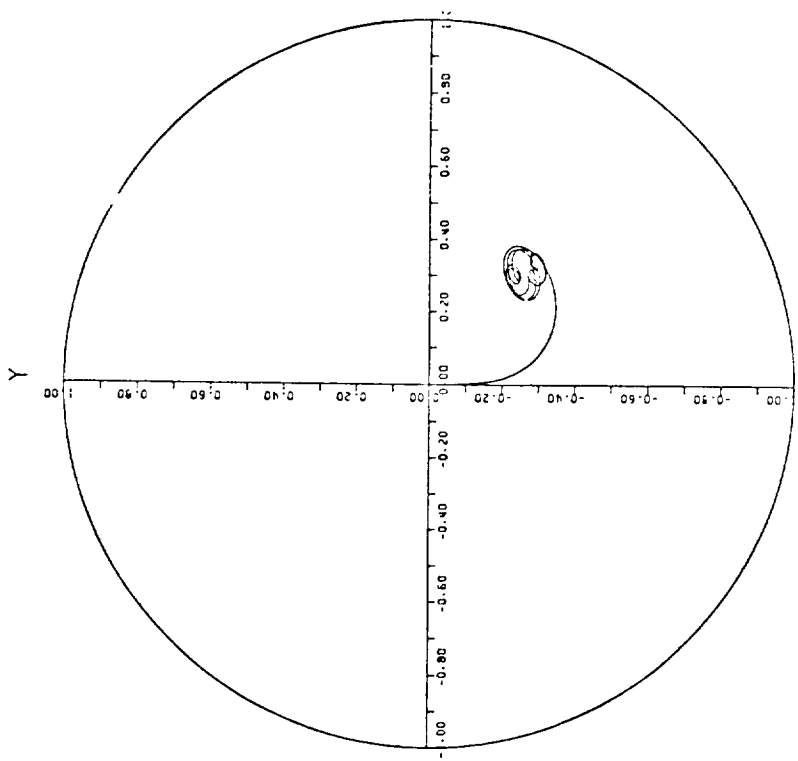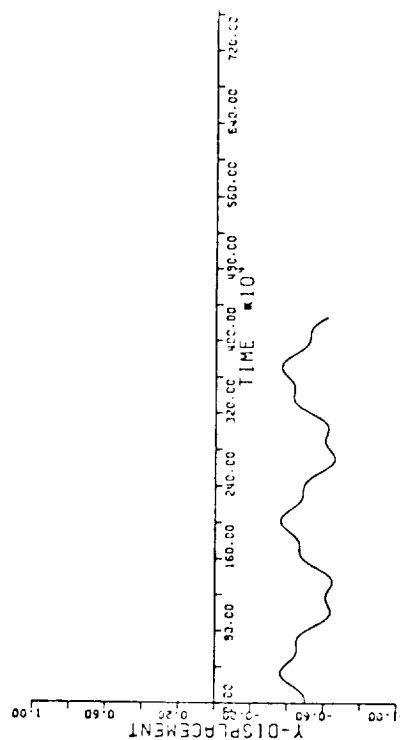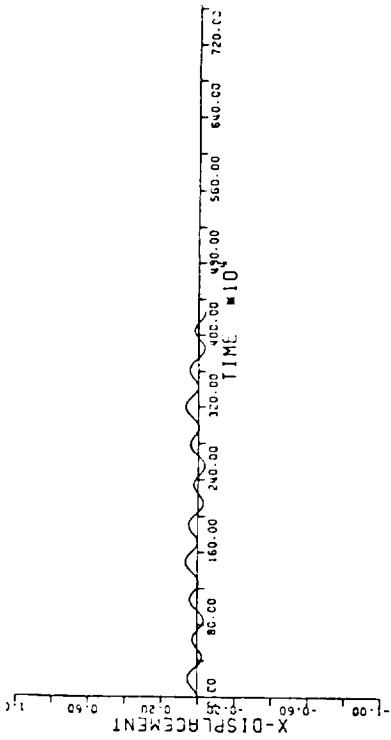
Figure 9. - Example of a flexible shaft with large unbalance.

343